

Occupied Electronic States of Li in Li, Li₂O₂, and Li₂O Analyzed by Soft X-ray Emission Spectroscopy

Keisuke Mukai,* Ryuta Kasada, Kazuya Sasaki, and Satoshi Konishi

Cite This: *J. Phys. Chem. C* 2020, 124, 9256–9260

Read Online

ACCESS |



Metrics & More

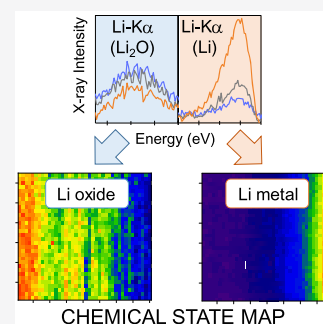


Article Recommendations



Supporting Information

ABSTRACT: Lithium metal and lithium oxides are components of lithium–oxygen (Li–O₂) batteries. To accurately identify Li compounds and understand the degradation mechanism, fundamental knowledge of the electron structures of constituent elements is vital. However, experimentally derived occupied states of Li have been missing due to the intrinsic difficulties in their detection. Herein, using soft X-ray emission spectroscopy, ultrahigh-energy-resolution spectra of Li–K were collected for three critical Li compounds: Li, Li₂O₂, and Li₂O. Large chemical shifts to lower energies and peak broadening were observed in compound-specific Li–K and O–K spectra. Theoretical calculations confirm that these changes derive from the characteristic electronic configurations of 1s and 2p states with core-level shifts in Li⁺. The large chemical shift (~4.6 eV) between the Li and Li₂O peaks was utilized to visualize the chemical state mapping of the Li metal/oxide phase, facilitating the identification of chemical phases in Li compounds.



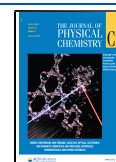
INTRODUCTION

Li–O₂ air batteries have attracted significant attention as alternative means of electrochemical storage because of their high specific energy densities.¹ In Li–O₂ cells, Li metal anode is oxidized and releases Li⁺ ions into the electrolyte on discharge; during charging, the process is reversed. Once Li⁺ is conducted through the electrolyte, it reacts with O₂^{2−} to form the final discharge product, lithium peroxide (Li₂O₂), at the cathode. The discharge product of lithium oxide, Li₂O, is also possible, which increases the specific energy stored, but reverse charging is hampered due to its insulating property.^{2,3} In addition to electrochemical storage, Li, Li-alloys, and lithium oxides can serve as intense neutron sources^{4,5} and tritium breeders in fusion reactors.^{6,7} Li metal and oxides are chemically reactive in ambient atmosphere to form impurity phases and corrosion products that can degrade the performance and raise safety concerns.^{8,9} The chemical phase analysis of Li-containing products contributes to our understanding of chemical reactions in the system. The chemical state distribution of Li compounds was previously reported using electron energy loss spectroscopy and Auger electron microscopy.^{10,11} Analysis of Li compounds is often hindered by (i) the low atomic number of Li (i.e., poor X-ray scattering power and extremely low photon energies at the K-edge), (ii) its high affinity to moisture resulting in compositional changes,^{12,13} and (iii) X-ray/electron irradiation-induced sample damage that occurs during characterizations. X-ray photoelectron spectroscopy (XPS) is a common technique used to obtain quantitative insights into core electrons, including Li 1s electrons.^{3,6,14} But, even with high-resolution XPS, Li 1s peaks overlap, as the shift of the binding energy is small compared to the energy resolution of XPS; a shift of less than 1.5 eV is observed for the Li 1s core levels between Li

metal and Li₂O.¹⁴ Thus, additional peak decompositions by fitting are required. Léon et al. investigated the valence electron structures of Li₂O and Li₂O₂ at the O K-edge using soft X-ray emission spectroscopy (SXES) at a synchrotron facility; the resulting spectra describe the valence electron structure of O.¹⁵ We note that Li valence electron structures must be determined experimentally for understanding the nature of chemical bonds and identifying oxide phases with Li. High-resolution K-edge spectral data can be exploited to visualize chemical state mapping on a microscopic scale, as demonstrated in our previous studies for Be (Z = 4) and B (Z = 5) compounds.^{16,17} Thus, in this study, the ultrahigh-energy-resolution (~0.2 eV) valence electron structures of Li in Li, Li₂O₂, and Li₂O were experimentally analyzed. We employ SXES with a highly sensitive X-ray charge-coupled device attached to an electron probe microanalyzer (EPMA).^{18,19} SXES is a bulk-sensitive measurement that covers ultrasoft X-rays in the energy range of 50–170 eV, including Li–K emission at 54.1 eV (i.e., 2p → 1s transition in Li). As the samples are metastable and may decompose during sample preparation or characterization, the obtained spectra are directly compared with the density of states (DOS) calculated using density functional theory (DFT) with all-electron configurations for Li (1s²2s¹). Due to large errors in band calculations in oxides,²⁰ not only a conventional functional

Received: April 1, 2020

Published: April 2, 2020



based on the generalized gradient approximation (GGA) but also a hybrid functional are utilized in this study. Finally, we show chemical state mappings of Li and Li_2O based on the knowledge of electron structures at the K-edge.

EXPERIMENTAL AND COMPUTATIONAL METHODS

Lithium metal rods (>99.9%, Mitsuwa Chemical Co., Ltd.), lithium peroxide (>99%, Kojundo Chemical Laboratory Co., Ltd.), and lithium oxide powders (>99%, Kojundo Chemical Laboratory Co., Ltd.) were analyzed. Li metal rod oxidation was carried out in air at 25 °C for 10 min; thereafter the sample was covered with the oxidized layer. Part of the surface layer was physically peeled off and the interface between the metal and oxide phases was analyzed by an area measurement using SXES. X-ray powder diffraction (XRD) was carried out in air using $\text{Co K}\alpha$ (RINT TTR-III, Rigaku) in the range of $2\theta = 10\text{--}80^\circ$ at intervals of 0.02° step. XRD data were analyzed using the RIETAN-FP program.²¹ The samples were analyzed by a JXA-8500F field emission EPMA using JEOL equipped with SXES (SS-94000SXES by JEOL). Sample powders were pressed on to a carbon tape mounted on the sample holder. The measurement time and the acceleration voltages of the electron beam were 60 s and 2.0 kV, respectively.

DFT calculations were performed using the Perdew–Burke–Ernzerhof (PBE) functional and HSE06 functional implemented in the Vienna ab initio simulation package (VASP).^{22–25} The electron configurations $1s^2 2s^1$ and $2s^2 2p^4$ were used for the Li and O atoms, respectively. The k -point meshes of $6 \times 6 \times 6$, $8 \times 8 \times 4$, and $6 \times 6 \times 6$ were generated using the Monkhorst–Pack scheme for the $2 \times 2 \times 2$ supercell of Li (cubic; $Im\bar{3}m$), $2 \times 2 \times 1$ supercell of Li_2O_2 (hexagonal; $P6_3mmc$), and $2 \times 2 \times 2$ supercell of Li_2O (cubic; $Fm\bar{3}m$), respectively. A plane-wave cutoff energy of 400 eV was used for calculations. Self-consistency was achieved with tolerance for a total energy of 10^{-5} eV, and the atomic positions were relaxed until the force was less than $0.02 \text{ eV } \text{\AA}^{-1}$. The energy of DOS was referenced to the Li 1s band centroid, $E_{\text{Li-1s}}$, $E_{\text{Li-1s}}$ was calculated as follows

$$E_{\text{Li-1s}} = \frac{\int_{-\infty}^{E_{\text{max}}} E g_{\text{Li-1s}}(E) dE}{\int_{-\infty}^{E_{\text{max}}} g_{\text{Li-1s}}(E) dE} \quad (1)$$

where $g_{\text{Li-1s}}(E)$ and E_{max} are the density of states of Li 1s orbitals at E and the maximum energy of the Li 1s orbitals, respectively.

RESULTS AND DISCUSSION

Li_2O_2 and Li_2O commercial powder samples were stored in an Ar-filled glove box and analyzed by XRD. Based on previous structural assessments of Li_2O_2 ,^{26,27} Rietveld refinements were carried out using the structure proposed by Föpl et al.²⁸ The results of multiphase Rietveld analysis (Figure S1 in the Supporting Information (SI)) showed minor peaks for LiOH ($P4/nmm$) in addition to the Li_2O_2 ($P6_3mmc$) and Li_2O ($Fm\bar{3}m$) phases. The Li_2O_2 and Li_2O powders contained ~ 6.3 and ~ 11.7 wt % LiOH as impurity phases, respectively, whereas no other impurity phase was found. Figure 1 shows Li DOS in Li, Li_2O_2 , and Li_2O using the PBE exchange–correlation functional and Heyd–Scuseria–Ernzerhof (HSE) hybrid functional. Figure 1a shows that the energetic difference in HSE between Li 1s centroid ($E_{\text{Li-1s}}$) and E_{F} in Li metal was

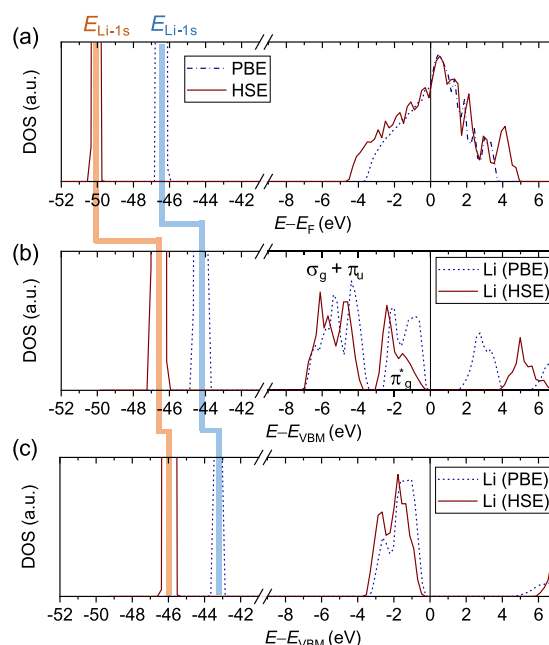


Figure 1. Electronic configurations of Li in Li (a), Li_2O_2 (b), and Li_2O (c) obtained by DFT using PBE and HSE. Orange and blue solid lines represent the positions of Li 1s centroid ($E_{\text{Li-1s}}$) and indicate core-level shifts of Li^+ .

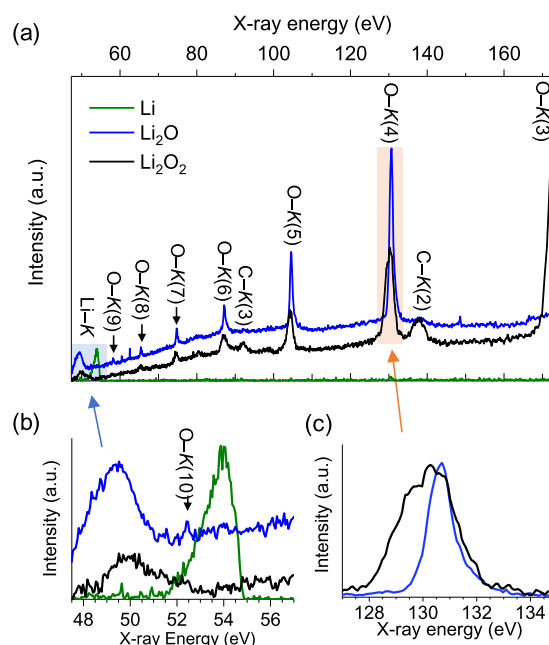


Figure 2. SXES spectra from the Li metal, Li_2O_2 , and Li_2O samples in the energy ranges of 47.5–173 eV (a), 47.5–57 eV for Li–K (b), and 127–135 eV for O–K(4) (c), in which the number in brackets denotes the X-ray diffraction order.

50.1 eV and had a significantly smaller error than that in PBE (46.4 eV). The value was nevertheless underestimated compared to the experimental value (54.1 eV). PDOS calculations for Li_2O_2 (Figure 1b) indicated valence electron states of Li^+ ions composing σ_g (bonding orbitals: p_z from -6.8 to -3.5 eV), π_u (bonding orbitals: p_x and p_y from -6.8 to -3.2 eV), and π_g^* (antibonding: p_x and p_y from -2.5 to 0 eV),²⁹ with a short gap approximately at -3.2 eV (Figures 1b and S2 in SI). The Li_2O band gap in PBE (4.9 eV) in Figure 1c was

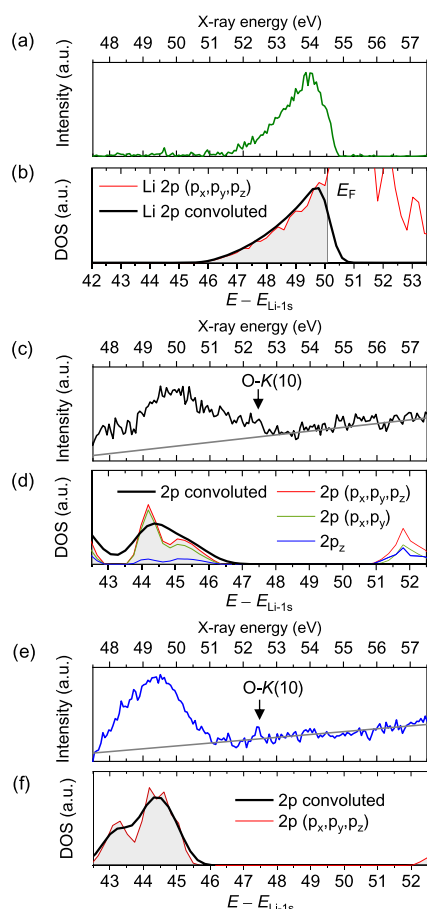


Figure 3. Experimental Li–K spectra for Li (a), Li_2O_2 (c), and Li_2O (e) using the SXES compared to the convoluted DOSs of occupied Li 2p states in Li metal (b), Li_2O_2 (d), and Li_2O (f) using HSE. The gray solid lines in panels (c) and (e) denote a linear background. The calculated energy is referenced to Li 1s centroid ($E_{\text{Li-1s}}$), where occupied Li 2p states below the Fermi energy and the VBMs are colored in gray. A comparison between the spectra and DOS using PBE is shown in Figure S3 in SI.

smaller than that in HSE (5.9 eV) and the experimental value (7.99 eV).³⁰ The energetic differences between $E_{\text{Li-1s}}$ and valence band maximum (VBM) in Li_2O_2 and Li_2O were -46.6 and -46.0 eV in HSE, respectively (Figures 1 and S3 in SI). These indicate core level shifts as large as 3.5 eV (Li_2O_2) and 4.1 eV (Li_2O) for Li^+ . These shifts are at least an order of magnitude higher than the SXES energy resolutions, indicating their applicability for chemical state mapping. The core electron state in Li_2O_2 was at least two times wider than

those in Li and Li_2O , due to the difference of electron structures at the two Li atom sites in Li_2O_2 (Figure S3 in SI). This can be a cause for the broad Li–K spectrum for Li_2O_2 .

Figure 2 shows the SXES spectra of the Li metal, Li_2O_2 , and Li_2O samples. In the obtained spectra, n th-order peaks for Li ($n = 1$) and O ($n = 3–10$) were observed; peaks of C ($n = 2$ and 3) were also observed due to the use of a carbon conduction tape. The Li–K spectrum of Li metal showed an asymmetric Doniach–Šunjić line shape in the range of 52–54.5 eV (Figure 2b). The Li–K peak intensities for Li_2O_2 and Li_2O were significantly lower than that for Li. Ionization to Li^+ causes numerous Li valence electrons to be lost and results in poor signal to noise (S/N) ratios. In Figure 3, the SXES Li–K spectra are directly compared with the DOS and PDOS of Li using HSE. The energy was referenced to $E_{\text{Li-1s}}$. The calculated Li 2p occupied states were convoluted, with Gaussian functions with full width at half-maxima (FWHM) of 0.6 eV (Li and Li_2O) and 0.9 eV (Li_2O_2) because of the difference in the 1s band width (Figure S3 in SI). The shapes of Li–K spectra agreed well with the convoluted 2p state. The calculated energies using HSE were estimated to be as large as 4.0 eV for Li metal and 5.3 eV for the oxides. A comparison between the experimental spectra and DOS using PBE (Figure S3 in SI) supports that the obtained spectral shapes describe Li valence electronic states. The Li–K spectrum for Li_2O_2 mainly derived from antibonding π_g^* orbitals appeared at 49–52 eV, while the peaks of bonding orbitals (σ_g and π_u) were below the SXES low-energy limit. However, the contributions of both bonding and antibonding orbitals can be seen in the broad peak of O–K(4) for Li_2O_2 in Figure 2c. The O–K(4) FWHM of the Li_2O_2 sample was 2.26 times wider than that of the Li_2O sample (Figure 2c), which was consistent with the valence band width ratio of 2.12 calculated using HSE (Figure 1b,c). The wide valence band was attributed to the anisotropic 2p states in Li_2O_2 (Figure S2 in SI). Although the unidentified O–K peak in Li_2O was observed at 528.9 eV in the previous SXES results,¹⁵ no peak was found at the corresponding position of 132.2 eV for O–K(4) in the Li_2O spectrum in the present work.

The chemical state and element mappings on a Li metal sample with a partial metallic surface that has been naturally oxidized in air are shown in Figure 4. The SXES spectra were collected at 40×32 measuring points (1280 points), with an acquisition time of 30 s per pixel (pixel size: $1 \times 1 \mu\text{m}^2$). From the naturally oxidized Li metal sample, the Li–K spectra of Li_2O ($E < 51$ eV) and Li (> 51 eV) were observed without peak overlap. No Li_2O_2 peak was found from the collected data, as predicted by the MALT thermodynamic database (Table S1 in SI). Chemical state mappings were constructed

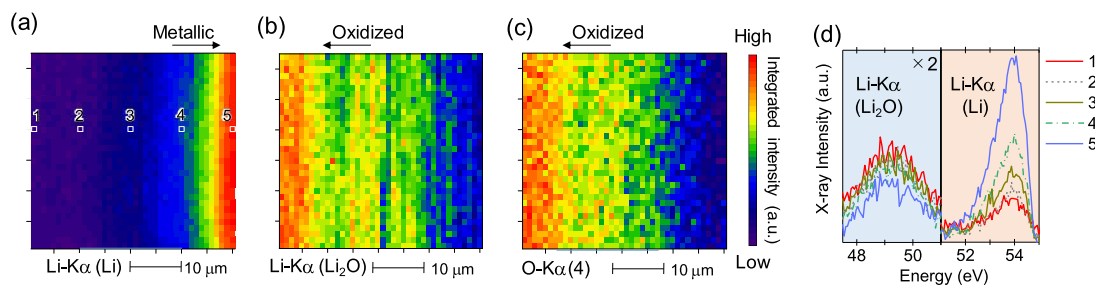


Figure 4. Chemical state mappings of Li metal ($E = 51.0–55.0$ eV) (a) and Li_2O ($E = 47.5–51.0$ eV) (b), element mapping of O using 4th order O–K ($E = 129–132$ eV) (c), and Li–K spectra at five measuring areas (d). Positions of the five measuring areas are shown in panel (a).

by calculating integrated intensities in the following energy ranges: Li_2O (47.5–51.0 eV) and Li metal (51.0–55.0 eV). Chemical state mappings (Figure 4a,b) visualize Li metal/oxide phase distribution on the sample; the metallic Li phase was distributed on the right side of the observed area, while the Li_2O phase lies on the left. Together with O element mapping (Figure 4c), it is possible to distinguish the Li_2O phase from other oxide phases lacking Li. To overcome weak Li–K emissions from oxide samples, an identification whether Li_2O_2 or Li_2O phase can be accomplished by integrating their antibonding orbitals appeared in the range of 128–130 eV for O–K(4) (Figure 2c).

CONCLUSIONS

The electron structures in Li metal, Li_2O_2 , and Li_2O were experimentally analyzed using soft X-ray emission spectroscopy. The chemical shifts of Li–K and peak broadening of Li_2O_2 O–K arose from Li core level shifts and characteristic 2p configurations, as confirmed by theoretical calculations using the hybrid functional. A large chemical shift (~ 4.6 eV) without peak overlap was utilized to visualize the chemical state mappings of Li and lithium oxide. The insights gained into Li electron structures are a basis for investigating the bond nature of Li and analyzing its chemical state, which could help further studies on controlling degradation processes.

ASSOCIATED CONTENT

Supporting Information

The Supporting Information is available free of charge at <https://pubs.acs.org/doi/10.1021/acs.jpcc.0c02885>.

Rietveld patterns of the X-ray diffraction data; DOS of the Li and lithium oxides using HSE, core electron states using HSE, and crystal structure of Li_2O_2 ; comparison between the experimental spectra and DOS using PBE; phase change of Li metal in air by thermodynamic calculations (PDF)

AUTHOR INFORMATION

Corresponding Author

Keisuke Mukai – Institute of Advanced Energy, Kyoto University, Uji, Kyoto 611-0011, Japan; orcid.org/0000-0001-8067-8732; Email: k-mukai@iae.kyoto-u.ac.jp

Authors

Ryuta Kasada – Institute for Material Research, Tohoku University, Sendai 980-8577, Japan

Kazuya Sasaki – Graduate School of Science and Engineering, Hirosaki University, Hirosaki, Aomori 036-8561, Japan; orcid.org/0000-0001-8510-0585

Satoshi Konishi – Institute of Advanced Energy, Kyoto University, Uji, Kyoto 611-0011, Japan

Complete contact information is available at: <https://pubs.acs.org/doi/10.1021/acs.jpcc.0c02885>

Notes

The authors declare no competing financial interest.

ACKNOWLEDGMENTS

This work is supported by the Joint Usage/Research Program on Zero-Emission Energy Research, Institute of Advanced Energy, Kyoto University (ZE29A-12, ZE30A-09, and ZE31A-24).

REFERENCES

- (1) Bruce, P. G.; Freunberger, S. A.; Hardwick, L. J.; Tarascon, J. M. Li–O₂ and Li–S batteries with high energy storage. *Nat. Mater.* **2012**, *11*, 19–29.
- (2) Zhang, S. S.; Foster, D.; Read, J. Discharge characteristic of a non-aqueous electrolyte Li/O₂ battery. *J. Power Sources* **2010**, *195*, 1235–1240.
- (3) Yao, K. P.; Kwabi, D. G.; Quinlan, R. A.; Mansour, A. N.; Grimaud, A.; Lee, Y. L.; Lu, Y. C.; Shao-Horn, Y. Thermal stability of Li_2O_2 and Li_2O for Li-air batteries: In situ XRD and XPS studies. *J. Electrochem. Soc.* **2013**, *160*, A824–A831.
- (4) Horiike, H.; Murata, I.; Iida, T.; Yoshihashi, S.; Hoashi, E.; Kato, I.; Hashimoto, N.; Kuri, S.; Oshiro, S. Liquid Li based neutron source for BNCT and science application. *Appl. Radiat. Isot.* **2015**, *106*, 92–94.
- (5) Kamada, S.; Takada, M.; Suda, M.; Hamano, T.; Imaseki, H.; Hoshi, M.; Fujii, R.; Nakamura, M.; Sato, H.; Higashimata, A.; Arai, S. Development of target system for intense neutron source of p-Li reaction. *Appl. Radiat. Isot.* **2014**, *88*, 195–197.
- (6) Tanaka, S.; Taniguchi, M.; Tanigawa, H. XPS and UPS studies on electronic structure of Li_2O . *J. Nucl. Mater.* **2000**, *283–287*, 1405–1408.
- (7) Mertens, M. A.; Aerts, A.; Infante, I.; Neuhausen, J.; Cottenier, S. Po-Containing Molecules in Fusion and Fission Reactors. *J. Phys. Chem. Lett.* **2019**, *10*, 2879–2884.
- (8) Wu, S.; Yi, J.; Zhu, K.; Bai, S.; Liu, Y.; Qiao, Y.; Ishida, M.; Zhou, H. A Super-Hydrophobic Quasi-Solid Electrolyte for Li–O₂ Battery with Improved Safety and Cycle Life in Humid Atmosphere. *Adv. Energy Mater.* **2017**, *7*, No. 1601759.
- (9) Park, C.; Nozawa, T.; Kasada, R.; Tosti, S.; Konishi, S.; Tanigawa, H. The effect of wall flow velocity on compatibility of high-purity SiC materials with liquid Pb–Li alloy by rotating disc testing for 3000 h up to 900 °C. *Fusion Eng. Des.* **2018**, *136*, 623–627.
- (10) Wang, F.; Graetz, J.; Moreno, M. S.; Ma, C.; Wu, L.; Volkov, V.; Zhu, Y. Chemical distribution and bonding of lithium in intercalated graphite: Identification with optimized electron energy loss spectroscopy. *ACS Nano* **2011**, *5*, 1190–1197.
- (11) Ishida, N.; Fukumitsu, H.; Kimura, H.; Fujita, D. Direct mapping of Li distribution in electrochemically lithiated graphite anodes using scanning Auger electron microscopy. *J. Power Sources* **2014**, *248*, 1118–1122.
- (12) Zhang, T.; Zhou, H. A reversible long-life lithium–air battery in ambient air. *Nat. Commun.* **2013**, *4*, No. 1817.
- (13) Terai, T.; Mohri, H.; Takahashi, Y. Equilibrium pressure of water vapor over a $\text{Li}_2\text{O}(\text{s})$ – $\text{LiOH}(\text{s,l})$ mixture. *J. Nucl. Mater.* **1991**, *179–181*, 808–811.
- (14) Wood, K. N.; Teeter, G. XPS on Li-battery-related compounds: analysis of inorganic SEI phases and a methodology for charge correction. *ACS Appl. Energy Mater.* **2018**, *1*, 4493–4504.
- (15) Léon, A.; Fiedler, A.; Blum, M.; Benkert, A.; Meyer, F.; Yang, W.; Bär, M.; Scheiba, F.; Ehrenberg, H.; Weinhardt, L.; Hesse, C. Valence Electronic Structure of Li_2O_2 , Li_2O , Li_2CO_3 , and LiOH Probed by Soft X-ray Emission Spectroscopy. *J. Phys. Chem. C* **2017**, *121*, 5460–5466.
- (16) Kasada, R.; Ha, Y.; Higuchi, T.; Sakamoto, K. Chemical State Mapping of Degraded B₄C Control Rod Investigated with Soft X-ray Emission Spectrometer in Electron Probe Micro-analysis. *Sci. Rep.* **2016**, *6*, No. 25700.
- (17) Mukai, K.; Kasada, R.; Yabuuchi, K.; Konishi, S.; Kim, J. H.; Nakamichi, M. Valence Electron and Chemical State Analysis of Be₁₂M (M = Ti, V) Beryllides by Soft X-ray Emission Spectroscopy. *ACS Appl. Energy Mater.* **2019**, *2*, 2889–2895.
- (18) Terauchi, M.; Takahashi, H.; Handa, N.; Murano, T.; Koike, M.; Kawachi, T.; Imazono, T.; Koeda, M.; Nagano, T.; Sasai, H.; Oue, Y.; et al. Ultrasoft-X-ray emission spectroscopy using a newly designed wavelength-dispersive spectrometer attached to a transmission electron microscope. *J. Electron Microsc.* **2012**, *61*, 1–8.
- (19) Takahashi, H.; Murano, T.; Takakura, M.; Asahina, S.; Terauchi, M.; Koike, M.; Imazono, T.; Koeda, M.; Nagano, T.

Development of soft X-ray emission spectrometer for EPMA/SEM and its application. *IOP Conf. Ser.: Mater. Sci. Eng.* **2016**, 109, No. 012017.

(20) Wang, L.; Maxisch, T.; Ceder, G. Oxidation energies of transition metal oxides within the GGA+ U framework. *Phys. Rev. B* **2006**, 73, No. 195107.

(21) Izumi, F.; Momma, K. Three-dimensional visualization in powder diffraction. *Solid State Phenom.* **2007**, 130, 15–20.

(22) Perdew, J. P.; Burke, K.; Ernzerhof, M. Generalized gradient approximation made simple. *Phys. Rev. Lett.* **1996**, 77, 3865–3868.

(23) Blöchl, P. E. Projector augmented-wave method. *Phys. Rev. B* **1994**, 50, 17953–17979.

(24) Kresse, G.; Furthmüller, J. Efficient iterative schemes for ab initio total-energy calculations using a plane-wave basis set. *Phys. Rev. B* **1996**, 54, 11169–11186.

(25) Heyd, J.; Scuseria, G. E.; Ernzerhof, M. Hybrid functionals based on a screened Coulomb potential. *J. Chem. Phys.* **2003**, 118, 8207–8215.

(26) Cota, L. G.; De La Mora, P. On the structure of lithium peroxide, Li_2O_2 . *Acta Crystallogr. B* **2005**, 61, 133–136.

(27) Chan, M. K.; Shirley, E. L.; Karan, N. K.; Balasubramanian, M.; Ren, Y.; Greeley, J. P.; Fister, T. T. Structure of lithium peroxide. *J. Phys. Chem. Lett.* **2011**, 2, 2483–2486.

(28) Föpl, H. Die Kristallstrukturen der Alkaliperoxyde. *Z. Anorg. Allg. Chem.* **1957**, 291, 12–50.

(29) Garcia-Lastra, J. M.; Bass, J. D.; Thygesen, K. S. Communication: Strong excitonic and vibronic effects determine the optical properties of Li_2O_2 . *J. Chem. Phys.* **2011**, 135, No. 121101.

(30) Ishii, Y.; Murakami, J.; Itoh, M. Optical Spectra of Excitons in Lithium Oxide. *J. Phys. Soc. Jpn.* **1999**, 68, 696.